A compact computational model for hyperthermia-controlled drug release based on Krogh-cylinder approach

Gabriele Adabbo[a,], Alberto Coccarelli[b,c], Marcello Iasiello[d], Assunta Andreozzi[d]*

[a]*Dipartimento di Medicina e Scienze della Salute "Vincenzo Tiberio", Università del Molise, Via Francesco De Sanctis 1, 86100, Campobasso, Italy.*

[b]*Zienkiewicz Institute for Modelling, Data and AI, Faculty of Science and Engineering, Swansea University, Swansea, UK.*

[c]*Department of Mechanical Engineering, Faculty of Science and Engineering, Swansea University, Swansea, UK.*

[d]*Dipartimento di Ingegneria Industriale, Università degli Studi di Napoli Federico II, P.le Tecchio 80, 80125, Napoli, Italy.*

**Corresponding author. Email: g.adabbo@studenti.unimol.it*

Keywords: Hyperthermia-mediated drug delivery, thermosensitive liposomes, 1D modeling, Krogh cylinder model

Abstract

Hyperthermia-mediated drug delivery offers a promising strategy to enhance the efficacy of chemotherapy while minimizing systemic toxicity. Thermosensitive liposomes (TSLs) release their therapeutic payload in response to elevated temperature, enabling targeted delivery to tumor tissues. Here we introduce a hybrid multiscale model based on a Krogh cylinder approach to describe temperature-sensitive liposome transport and drug release in tumor tissue. Spatial transport of liposomes and released drug in the vascular and interstitial domains is described by one- dimensional (1-D) transport equations, while intracellular drug internalization is represented by local compartmental (0-D) kinetics. The model incorporates key physiological processes including blood flow, passive transvascular diffusion of liposomes, interstitial diffusion of released drug, and cellular uptake via receptor binding and internalization. The temperature field is calculated using the Pennes' bioheat equation, and its effects on physiological parameters - such as permeability, diffusivity, and blood velocity - are incorporated via temperature-dependent functions. A sensitivity analysis was performed to identify dominant transport parameters. Microvascular permeability, tissue diffusivity and Krogh cylinder radius were identified as the most influential parameters affecting drug delivery. Simulation results revealed that a 30-minute preheating phase prior to drug administration significantly enhances treatment efficacy, increasing internalized doxorubicin concentrations by 29.4% while maintaining a low probability (5%) of tissue necrosis.

This compact and computationally efficient model provides an effective framework for designing and optimizing hyperthermia-assisted chemotherapy. Its computational efficiency and physiological detail make it specifically suitable for use in treatment planning and real-time therapeutic decision-making in solid tumors.

Nomenclature

Latin symbols	Description	Units
A	Frequency factor for thermal damage	s^{-1}
A_1, A_2	Coefficients in plasma concentration input function	$mol \cdot m^{-3}$
c	Specific heat capacity of tissue	$J \cdot kg^{-1} \cdot K^{-1}$
c_B	Specific heat capacity of blood	$J \cdot kg^{-1} \cdot K^{-1}$
C_{rec}	Tumor cell receptor concentration	$mol \cdot m^{-3}$
C^t_L	Tissue concentration of liposomes	$mol \cdot m^{-3}$
C^v_L	Vascular concentration of liposomes	$mol \cdot m^{-3}$
C_{dox}	Tissue concentration of doxorubicin	$mol \cdot m^{-3}$
C_B	Concentration of bound drug	$mol \cdot m^{-3}$
C_I	Concentration of internalized drug	$mol \cdot m^{-3}$
D_L	Diffusion coefficient of liposomes in tissue	$m^2\ s^{-1}$
D_{dox}	Diffusion coefficient of doxorubicin in tissue	$m^2\ s^{-1}$
ΔE	Activation energy for thermal damage	$J \cdot mol^{-1}$
k_1, k_2	Time constants in plasma concentration function	s^{-1}
k_b	Boltzmann constant	$J\ K^{-1}$
k_{int}	Internalization rate constant	s^{-1}
k_{off}	Drug-receptor dissociation rate	s^{-1}
k_{on}	Drug-receptor binding rate	$m^3 \cdot mol^{-1} \cdot s^{-1}$
k_{rel}	Temperature-dependent drug release rate	s^{-1}
L	Krogh cylinder length	m
n_c	Number of Krogh cylinders	–
P	Microvascular permeability	$mm\ s^{-1}$
q_p	Transvascular flow	$mol \cdot m^{-3} s^{-1}$
R	Krogh cylinder outer radius	m
R_g	Universal gas constant	$J \cdot mol^{-1} K^{-1}$
r_c	Capillary radius	μm
r	Radial coordinate	m

S/V	Surface area to volume ratio of vasculature	m^{-1}
T	Temperature	°C
T_B	Blood temperature	°C
T_0	Initial temperature	°C
u	Blood flow velocity	mm s^{-1}
V_t	Volume of solid tissue	m^3
x, z	Spatial coordinates	m
Greek symbols	**Description**	**Units**
γ	Fraction of tumor volume accessible to drug	–
θ	Probability of thermal damage	–
ξ	Blood velocity temperature coefficient	$°C^{-1}$
ρ	Tissue density	$kg \cdot m^{-3}$
ρ_B	Blood density	$kg \cdot m^{-3}$
τ	Time integration constant	s
χ	Perfusion temperature coefficient	$°C^{-1}$
ψ	Permeability temperature coefficient	$°C^{-1}$
ω	Blood perfusion rate	s^{-1}
ω_0	Baseline blood perfusion rate	s^{-1}
Abbreviations		
0-D	Zero-dimensional (lumped model)	–
1-D	One-dimensional	–
3-D	Three-dimensional	–
Bi	Biot number	–
LHS	Latin Hypercube Sampling	–
SAR	Specific Absorption Rate	$W \cdot m^{-3}$
SRRC	Standardized Ranked Regression Coefficient	–

1. Introduction

Although chemotherapy represents a fundamental cornerstone of cancer treatment; its systemic administration, especially with drugs like doxorubicin, poses significant challenges in managing side-effects. Due to their cytotoxic nature, traditional chemotherapeutic agents do not differentiate between cancerous and healthy cells, often leading to severe side effects such as immune suppression, inflammation, and damage to mucosal tissues [1]. Thermal treatments, when used alongside radiotherapy or chemotherapy, have emerged as promising strategies for treating different types of

cancers [2][3]. A particularly innovative approach in drug delivery involves thermo-sensitive liposomes (TSLs) [4], [5], which are lipid-based nanoparticles engineered to release their therapeutic payload in response to mild heat exposure. This targeted delivery system enhances drug accumulation in tumor cells while significantly reducing damage to surrounding healthy tissues, thereby improving the efficacy and safety of chemotherapy. This approach employs externally applied heat to trigger the release of therapeutic agents from the temperature-sensitive carriers, thereby improving drug penetration and uptake in malignant tissues [6].

From a clinical perspective, computational modelling can aid in designing hyperthermia regimens to optimize drug delivery and in their real-time adjustment during therapy. During hyperthermia, the delivery and activation of liposomes and their payload from the bloodstream to tumor cells are governed by the kinetics of mass transport across the vascular wall and within the surrounding tissue. Models that explicitly account for spatial transport allow to capture the timing of drug distribution and the resulting concentration gradients within the tissue, both of which critically influence therapeutic effectiveness.

High-fidelity 3D models [7], [8], [9], [10] offer detailed spatial resolution, but their high computational cost limits their use in clinical settings for treatment planning and optimization. On the other hand, lumped-parameter or compartmental (0-D) models, such as [11], are computationally inexpensive but treat the tumor as a well-mixed compartment, thereby losing critical information about drug diffusion gradients and penetration depth within the tissue.

To address the limitations of these approaches, we propose a new spatially and temporally resolved computational framework based on the Krogh cylinder model for evaluating temperature-controlled drug distribution within the tumor microenvironment. The Krogh cylinder model has been widely employed for the simulation of oxygen diffusion from capillaries into surrounding tissue [12], and for drug delivery [13], but it has not been yet employed in the context of thermal therapies. The present framework incorporates a description of blood flow using an equivalent capillary model (which represents the microvascular network), the passive diffusion of drugs through the vascular wall, and their subsequent distribution within the tumor tissue. Drug concentration in the tissue compartment and the binding and internalization phenomena at the cellular level are simulated using a three-compartment model. By coupling these processes with the Pennes' bioheat equation (widely employed in bioheat models [14]) for the evaluation of the temperature level in order to trigger the drug release from the TSL, the model captures the influence of temperature on drug release dynamics, enabling an assessment of treatment efficacy under different heating protocols.

The novelty of this work lies in bridging this gap: we present a 1-D radially resolved framework that couples blood flow with interstitial transport. This approach retains the spatial fidelity necessary to

predict drug penetration depth while achieving the computational efficiency required for extensive global sensitivity analysis and potential real-time clinical application. A key focus of this work is the evaluation of temperature-dependent physiological parameters - such as microvascular permeability, blood velocity, and diffusivity - and their impact on drug distribution across the blood and tumor tissue. Through sensitivity analysis, we identify the critical factors that govern drug transport and highlight the potential benefits of a preheating strategy to enhance drug delivery efficiency. The findings of this study provide valuable insights into the optimization of hyperthermia-assisted chemotherapy and contribute to the development of more effective treatment strategies for solid tumors.

2. Methods

The scales of the proposed hybrid (1-D-0-D) modelling framework are depicted in Figure (1), while the described processes are (i) the transport of a liposome-encapsulated drug from the arterial circulation to solid tissue, (ii) heat-induced drug release from liposomes into the extracellular space, and (iii) drug binding and internalization by cancerous cells. In this study, we consider doxorubicin encapsulated within thermo-sensitive liposomes; however, the same modeling framework can be applied to other agents administrated into the bloodstream. It is assumed that liposomes distribute across the vascular wall and surrounding tissue via passive diffusion. Induced hyperthermia triggers the release of encapsulated doxorubicin from liposomes, which binds to receptors on nearby tumor cells and is subsequently transferred into the intracellular space. Since this therapeutic strategy is mainly employed in the treatment of liver solid tumors such as hepatocellular carcinoma, we consider model parameters that are representative of this type of tissue and associated vasculature.

The assumptions and governing equations describing these processes underlying the selected thermal therapy are reported in the following sections.

Since this therapeutic strategy is mainly employed in the treatment of liver solid tumors such as hepatocellular carcinoma, we consider model parameters that are representative of this type of tissue and associated vasculature.

2.1 Liposomal transport in the blood stream

The Krogh cylinder model has been largely employed, in simulating oxygen transport and diffusion in tissues [15], and here is used to describe the transport of liposomes from the blood to the tissue compartment. Tumor microvasculature consists of an intricate network of microvessels (arterioles,

capillaries and venules) which supply oxygen and nutrients to the surrounding (tumor) tissue. Microvessels feeding tumor regions exhibit higher levels of tortuosity and are leakier than in healthy tissue [16], which may lead to local heterogeneities in the solute tissue concentration. Since we focus on optimizing the timing of the therapeutic intervention, here we adopt a simplified approach to describe the blood-tissue spatial interface (Figure 1). A volume of solid tissue V_t with embedded microvasculature can be represented by n_c equal Krogh cylinders, defined by an axial length L, an inner radius r_c and outer radius R (see Figure 1c). The total blood flow supply to the tissue volume is equally distributed between the n_c cylinders, which act as flow resistances in parallel.

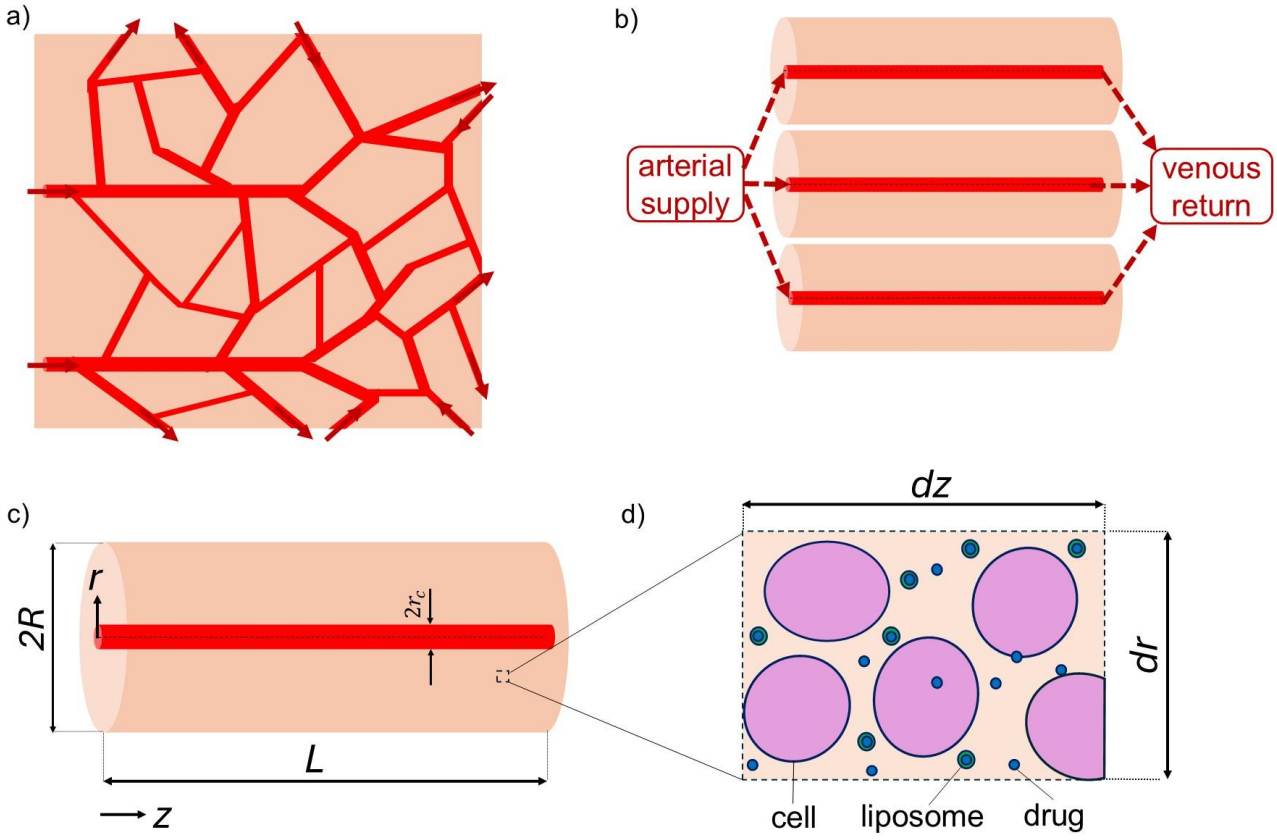

Figure 1: Hybrid Krogh-cylinder transport model: a) microvascular network embedded within tissue (red arrows indicate blood flow direction); b) blood-tissue spatial organization using Krogh cylinder approach; c) dimensions of the Krogh cylinder; d) liposome and drug distribution within tissue.

Each Krogh cylinder contains an equivalent (straight) capillary running along its axial direction, representing the bloodstream that supplies the tissue within it. The axial length of the cylinder L is chosen to represent the average path length undertaken by liposomes from arterial to venous circulation, while the outer radius R reflects the volume of tissue that is supplied by one capillary, and can be interpreted as the inverse of capillary density (per tissue volume) [15].

The radius of the capillary r_c is set to be equal to 5.0 μm, which is a typical value for the liver sinusoids [17]. Although the capillary radius (5 μm) is smaller than the diameter of red blood cells (RBCs), the

resulting single-file transport induces a “bolus flow” regime. This phenomenon generates strong mixing eddies within the plasma gaps between RBCs, effectively homogenizing the drug concentration radially across the vessel cross-section. Consequently, the assumption of uniform vascular concentration dependent only on the axial position (z) is physically justified. Furthermore, the blood flow velocity is treated as a time-average bulk parameter, smoothing out the discrete nature of RBC passage to suit the continuum mechanics of the Krogh framework.

This geometrical configuration is employed to describe the transport of thermosensitive liposomes across microcirculation. The solute is advected by blood along the equivalent capillary and diffuses radially through the vascular wall. The concentration of loaded liposomes in plasma C_L^v varies in time and along the capillary bed according to the following equations:

$$\frac{\partial C_L^v}{\partial t} + u\frac{\partial C_L^v}{\partial z} = -q_p \tag{1}$$

$$q_p = P(T)\frac{S}{V}(C_L^v - C_L^t) \tag{2}$$

where u is the average blood flow velocity and C_L^t represents the (loaded) liposomal concentration in the surrounding tissue space. This approach is based on the methodology used in [15]. Here, P (mm s^{-1}) refers to the microvascular permeability of the vascular compartment, which is assumed to be temperature-dependent, while S/V (m^{-1}) represents the ratio of the vascular compartment surface area to its volume, which is estimated to be equal to $2/r_c$ (where r_c is the equivalent capillary radius). The interaction between blood and tissue compartments is represented by the liposomal extravasation term q_p in Equation (1), which corresponds to a source term in the tissue diffusion equation (shown in section 2.2). Convective transport of the solute through the vascular wall is assumed negligible due to the high interstitial pressure typically observed in tumors, which restricts fluid movement [18]. Consequently, the model only accounts for passive diffusion across the vascular wall, since the intracapillary pressure is nearly equal to the interstitial pressure [19]. The solute plasma concentration at inlet is based on experimental data from [20], similar to the approach adopted in a previous reference work [10]. This time-dependent function reads:

$$c_{in}(t) = A_1 \exp(-k_1 t) + A_2 \exp(-k_2 t) \tag{3}$$

2.2 Liposomal tissue transport, drug release and internalization

In this study, the solid tissue is represented as a single-phase medium, and solute diffusion along the axial direction of the cylinder is considered negligible. After crossing the vascular wall, loaded liposomes accumulate and diffuse radially through the surrounding cylindrical tissue. Once these are exposed to mild hyperthermia, their membrane permeability increases substantially, allowing the release of the drug payload (in this study, doxorubicin). The concentration of loaded liposomes within the tissue is governed by the following equation:

$$\frac{\partial C_L^t}{\partial t} = D_L(T)\ \frac{1}{r}\frac{\partial}{\partial r}\ \left(\frac{\partial C_L^t}{\partial r}\right) - k_{rel}(T)C_L^t + q_p \tag{4}$$

where $D_L(T)$ and $k_{rel}(T)$ are the liposomal diffusion coefficient in tissue and drug release rate, respectively. Both terms are temperature-dependent and are discussed in Section 2.3. In Equation (4), thermally-activated liposomes are removed from the mass balance, while the liposomal extravasation term is non-zero only at the interface between the tissue and the bloodstream ($r = r_c$).

The drug released in the extracellular space by hyperthermia accumulates, diffuses (radially) across the tissue and interacts with cancer cells' receptors. The time- and space-dependent variation of the drug concentration in the tissue C_{dox} is described via the following:

$$\frac{\partial C_{dox}}{\partial t} = D_{dox}(T)\ \frac{1}{r}\frac{\partial}{\partial r}\ \left(\frac{\partial C_{dox}}{\partial r}\right) + k_{rel}(T)C_L^t - \frac{1}{\gamma}k_{on}C_{rec}C_{dox} + k_{off}C_B \tag{5}$$

where $D_{dox}(T)$ is the drug tissue diffusivity (temperature-dependent, discussed in Section 3.3), C_{rec} is the concentration of tumor cell receptors, C_B is the concentration of bound drug (to the cell receptors), γ is the fraction of tumor volume accessible to drugs, while k_{on} and k_{off} are the drug-receptor association and dissociation kinetic constants, respectively. The parameters values are taken from [21].

A symmetry (no flux) boundary condition is imposed at the outer radius of the Krogh cylinder for both liposome and doxorubicin concentrations, assuming that the solid tissue consists of numerous packed identical cylinders, such that $\frac{\partial C_L^t}{\partial r}|_{r=R} = 0$, and $\frac{\partial C_{dox}^t}{\partial r}|_{r=R} = 0$. While at the capillary interface ($r = r_c$) the mass flux is governed by passive diffusion $-D_L\frac{\partial C_L^t}{\partial r}|_{r=r_c} = P(T)\frac{S}{V}(C_L^v - C_L^t)$.

The binding and internalization of the anti-cancer drug to tumor are locally evaluated (at each tissue radial coordinate) through the following ordinary differential equations:

$$\frac{dC_B}{dt} = \frac{1}{\gamma} k_{on} C_{rec} C_{dox} - (k_{off} + k_{int}) C_B \quad (6)$$

$$\frac{dC_I}{dt} = k_{int} C_B \quad (7)$$

where C_I is the concentration of internalized drug in the tumor cells, and k_{int} the constant of internalization rate. The mathematical framework formed by Equations (4-7) has previously been used successfully to simulate hyperthermia-mediated drug delivery, both in 0-D compartmental models [21], and for 3-D applications [9].

2.3 Temperature evolution and effect in tissue

The temperature evolution resulting from external heating is modeled using the lumped parameter Pennes' bioheat equation [22]:

$$\rho c \frac{dT}{dt} = \dot{Q} - \omega(T) \rho_B c_B (T - T_B) \quad (8)$$

Notably, since the purpose of this work is not to simulate the electromagnetic field generated by the microwave treatment, a constant value is assumed for the heat generation resulting from resistive losses in the tissue. This assumption simplifies the model without significantly affecting accuracy, as the lumped parameter approximation for the energy equation is considered reliable due to the small size of the domain. Specifically, by assuming a blood velocity of 0.2 mm s^{-1} (which is a reliable assumption for liver sinusoids [23]), it is possible to consider a convective heat transfer coefficient of 170 W $m^{-2}K^{-1}$ [24], lower than the one measured and, therefore, a Biot number equal to 2.59e-3, much lower than 0.1, suggests the reliability of the lumped parameter model [25].

The release of doxorubicin depends on the function $k_{rel}(T)$ (measured in s^{-1}), which is a temperature-dependent parameter. In the present model, this function is defined as a piecewise function, following the methodology described in [26].

$$k_{rel}(T) = \begin{cases} 0 & if \quad T < 42°C \\ 0.114 & if \quad T \geq 42°C \end{cases} \quad (9)$$

The diffusion coefficients for liposomes and drug in tissue are assumed to be linearly dependent on temperature via the Einstein-Stokes equation: $D = \frac{k_b T}{6\pi\eta r}$, where k_b is the Boltzmann constant, T the absolute temperature, η the fluid viscosity and r the mean radius of the spherical particles (for TSLs it is approximately equal to 50 nm). The latter is valid for particles diffusing in a low Reynolds flow.

Furthermore, several parameters within the present model are assumed to be temperature-dependent in order to capture the effects of temperature on the drug delivery process. These parameters include the permeability of the vessel wall, the diffusion coefficients of both liposomes and doxorubicin, the blood perfusion rate, and the blood velocity. Although no explicit analytical functions for all the set of parameters are available in the literature to describe how these change with temperature, there are descriptions indicating how their values increase with rising temperature. Therefore, in this work, we adopt a linear function to describe the temperature dependence of these parameters. In particular, for the perfusion rate, a 2-folds linear increase up until 42°C [27], before vascular stasis [28], is considered.

$$\omega(T) = \omega_0[1 + \chi(T - T_B)] \tag{10}$$

with χ = 0.2 °C^{-1} and T_B equal to 37°C as reference temperature for blood. For the baseline value, a volume flow rate for the liver equal to 1000 l min^{-1} [29] is assumed, considering a total liver volume of 1500 cm^3 [30], the overall baseline perfusion rate is equal to ω_0 = 0.011 s^{-1}. Similarly, a linear temperature dependency is applied to the permeability coefficient and the blood velocity. Based on experimental data, microvessel permeability during hyperthermia treatment has been observed to increase by a factor of 5 to 17 times [31], [32], For this work, we assume an average increase of 9-fold between 37°C and 42°C. The increase in blood velocity is also assumed to follow the behavior of the perfusion rate.

$$P(T) = P_0[1 + \psi(T - T_B)] \tag{11}$$

$$u(T) = u_0[1 + \xi(T - T_B)] \tag{12}$$

Equations (11) and (12) express the linear temperature dependence of permeability and blood velocity, where ψ = 1.6 °C^{-1} and ξ = 4e-4 °C^{-1}. The permeability baseline value is the one considered for 37°C equal to 3.4e-3 μm s^{-1} [33].

2.4 Solution procedure

All parameters' value employed for the simulations are resumed in Table 1.

Table 1: Thermophysical parameters values employed in the simulations.

Parameter	Value	Reference
P_0 ($\mu m\ s^{-1}$)	3.4e-3	[33]
u_0 ($mm\ s^{-1}$)	0.2	[23]
D_L(T = 37°C) ($\mu m^2\ s^{-1}$)	9.0	[8]
D_{dox}(T = 37°C) ($\mu m^2\ s^{-1}$)	160.0	[11]
k_{on} ($m^3\ mol^{-1} s^{-1}$)	1.5e6	[21]
k_{off} (s^{-1})	8.0e-3	[21]
C_{rec} ($mol\ m^{-3}$)	1.0e-5	[21]
γ (-)	0.3	[21]
ω_0 (s^{-1})	0.011	estimated
k_{int} (s^{-1})	5.0e-5	[21]
ρ ($kg\ m^{-3}$)	1045	[34]
c ($J\ kg^{-1} K^{-1}$)	3760	[34]
ρ_B ($kg\ m^{-3}$)	1050	[34]
c_B ($J\ kg^{-1} K^{-1}$)	3693	[34]
A_1 ($mol\ m^{-3}$)	0.012	[11]
A_2 ($mol\ m^{-3}$)	0.021	[11]
k_1 (s^{-1})	8.37e-5	[11]
k_2 (s^{-1})	4.17e-6	[11]

The governing equations are solved through finite difference discretization method, in particular a first-order backward difference scheme for the convection equation (Equation 1) and a second-order central difference scheme for the diffusion equations (Equations 4-5). Backward Euler is employed for the implicit time discretization. The structured mesh consists of 20 nodes on the z-axis and 15 on the r-axis. The chosen time step is equal to 1.0 second, due to the intrinsic stability of the implicit time-stepping scheme. The initial value for liposomes' concentration within the tissue is fixed equal to zero, while the initial temperature is equal to 37°C all over the domain.

2.5 Comparison with 0-D compartmental model

To effectively test the reliability of the present 1-D model, we compare the results for nanoparticles concentration in the solid tissue with those obtained by El-Kareh and Secomb [11] using a lumped

parameter model. For this simulated case, the Krogh cylinder radius and length are assumed equal to 50 μm [15] and 900 μm [35], respectively. The results are compared with the analytical solution to the partial differential equation (Equation 13), since a direct comparison with experimental data is challenging due to the high specificity of the theoretical application under study. The comparison results are displayed in Figure 2.

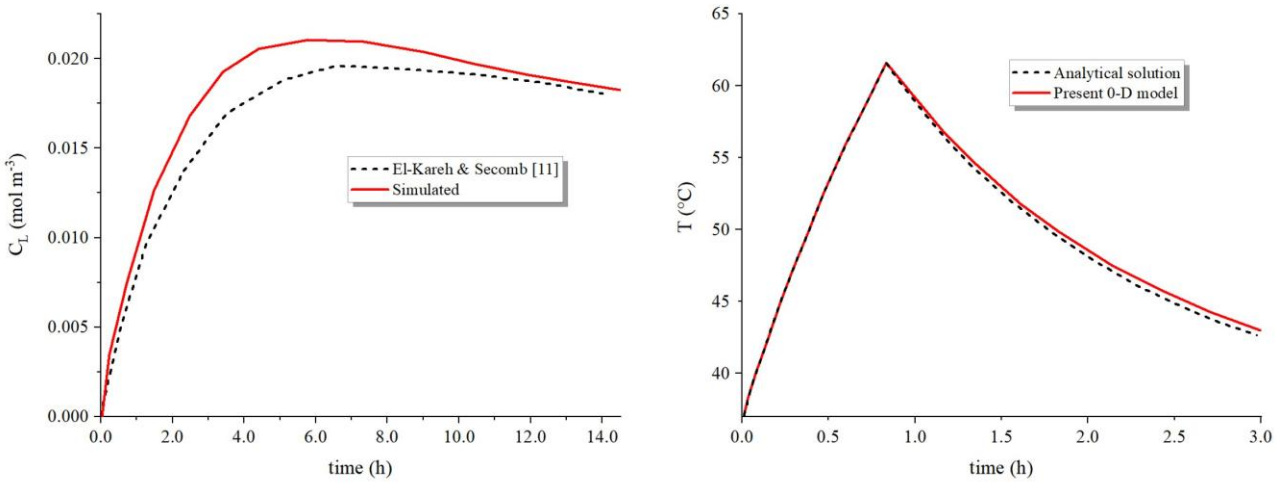

Figure 2: Left panel: liposomes concentration in tissue comparison with the 0D model presented in *[11]*. Right panel: bioheat model comparison with analytical solution, eq (13).

The bioheat model (Equation 8) assumed a heat generation $\dot{Q}$ = 2.5e6 W m^{-3}, which is typical SAR value obtained in tumoral tissue with the here employed thermophysical properties when a microwave heating with a 5 W inlet power is performed, measured in the proximity of the antenna [9]. To capture the time-dependent heating process, the equation has been solved by considering 60 seconds in which the heat generation is on, followed by a 120 second cooling. The initial temperature for the bioheat model T_0 is fixed at 37°C.

$$T(t) = \begin{cases} \frac{1}{\omega\rho_B c_B}\left(\frac{\dot{Q}}{\rho c} + \omega\rho_B c_B T_B\right) + \left(T_0 - \frac{1}{\omega\rho_B c_B}\left(\frac{\dot{Q}}{\rho c} + \omega\rho_B c_B T_B\right)\right) e^{-\omega\rho_B c_B t}, & t \le t^* \\ T_0 + (T(t^*) - T_0) e^{-\omega\rho_B c_B (t - t^*)}, & t > t^* \end{cases} \quad (13)$$

For comparison purposes, when comparing with the analytical solution, the blood perfusion rate is held constant and assumed to be independent of temperature. This simplification facilitates comparisons and aligns the bioheat model with the assumptions made in the analytical solution.

3. Results and discussion

3.1 Impact of mass transport parameters on drug concentration

The objective of this study is to investigate how to improve and optimize this kind of treatment from a computational point of view with the employment of a computationally efficient numerical model, one of the optimization procedure tested in the present work regards the preheating of the interested tissue, in order to assess if the temperature dependence of the involved physiological parameters could improve the final therapeutic goal. It is necessary, in this context, to assess the influence of the key physiological parameters involved on drug mass transfer from bloodstreams to cancer cells. To achieve this, a sensitivity analysis has been conducted on the key parameters of the model. This analysis aims to quantify the impact of each parameter on drug transport and uptake by the tissue. The parameters selected for the sensitivity analysis include the length and radius of the Krogh cylinder, blood velocity, the diffusivity coefficient of the nanoparticles, and the microvascular permeability. The effect of each of these parameters is assessed based on four target functions: (1) the maximum liposomes concentration achieved within the tissue, (2) the total mass exchange between the blood and tissue domains, (3) the maximum concentration of bound drug, and (4) the maximum concentration of internalized drug. To carry out the sensitivity analysis, the Standardized Ranked Regression Coefficient (SRRC) for each parameter has been calculated, providing a measure of the relative influence of each variable on the model outcomes. Initially, the model was executed using a Latin Hypercube Sampling (LHS) method, which allows for an efficient exploration of the parameter space by treating each parameter as variable within a predefined range. Within these ranges, *n* values are samples between the minimum and maximum limits, ensuring thorough coverage across the range. The specific variability ranges for each parameter, which define the bounds within which each parameter can fluctuate, are presented in Table 2.

Table 2: Variability range for the parameters employed in the sensitivity analysis. *The parameter "k_{on}" quantifies the binding capability of doxorubicin to tumor cells, thus, it is employed only to assess its influence on bound and internalized drug concentrations.

Parameter	**Range** *(starting value : final value : n)*
L (m)	5.0e-4 : 5.0e-3 : 20
R (m)	5.0e-6 : 5.0e-4 : 20
D_0 ($m^2\ s^{-1}$)	9.0e-13 : 9.0e-11 : 20
P_0 ($m\ s^{-1}$)	3.4e-10 : 3.4e-8 : 20
u_0 ($m\ s^{-1}$)	2.0e-5 : 2.0e-2 : 20
k_{on} ($m^3\ mol^{-1} s^{-1}$)*	1.0e-1 : 1.0e6 : 20

The parameter ranges detailed in Table 2 represent physiological limits defined by the heterogeneous nature of solid tumors rather than arbitrary numerical bounds. Regarding geometry, the Krogh cylinder radius (R) was varied from 5 to 500 μm to probe the limits of therapeutic efficacy in poorly vascularized regions. While functional inter-capillary distances in viable tumor rims are typically short, extending the upper bound to 500 μm allows the model to simulate hypoxic and semi-necrotic cores where the distance from the nearest vessel significantly exceeds the diffusion limit of oxygen (~150 μm) [3]. Similarly, the cylinder length (L) was varied from 0.5 to 5 mm to account for different levels of vascular tortuosity.

In parallel, hemodynamic and transport parameters were selected to reflect the chaotic nature of tumor perfusion. The microvascular permeability (P_0) range spans two orders of magnitude to capture structural diversity, ranging from vessels with tight junctions to those exhibiting large fenestrations associated with the Enhanced Permeability and Retention (EPR) effect [4]. Likewise, the blood velocity range is sufficiently broad to encompass regimes of vascular stasis caused by high interstitial fluid pressure as well as high-velocity arteriolar shunts [5]. Finally, the binding rate constant (k_{on}) was varied across orders of magnitude to mechanistically delineate the transition from reaction-limited (low affinity) to diffusion-limited (high affinity) uptake, ensuring that the identification of transport barriers remains robust across physiological conditions.

LHS is a typology of stratified Monte Carlo sampling that divides the range of the K parameters included in the analysis ($Y_1, Y_2, \ldots, Y_K$) into N intervals. In such a way, the probability of the variable falling in any of the intervals is $1/N$. The value selection from each interval is randomly performed, and the N values assigned to the Y_1 variable are randomly paired with the N values of the second variable Y_2, and furthermore combined with the N values of the third one, and so on. Finally, the domain results in N combinations of the K variables which is the sample used for the sensitivity analysis. In the present study, to analyze monotonic non-linear correlations, the Standardized Ranked Regression Coefficient (SRRC) is employed. SRRCs are selected as sensitivity indices because, varying from -1 to 1, exhibit how influential are the input parameters on the output functions. Negative values refer to the opposite variation between input and output, while positive values represent a concordant variation. The magnitude of the influence – growing from 0 to 1 – is estimated to assess how the variation of the treated parameters affects the output functions. In Figure 3, the histogram representation of the SRRCs for the considered parameters is shown.

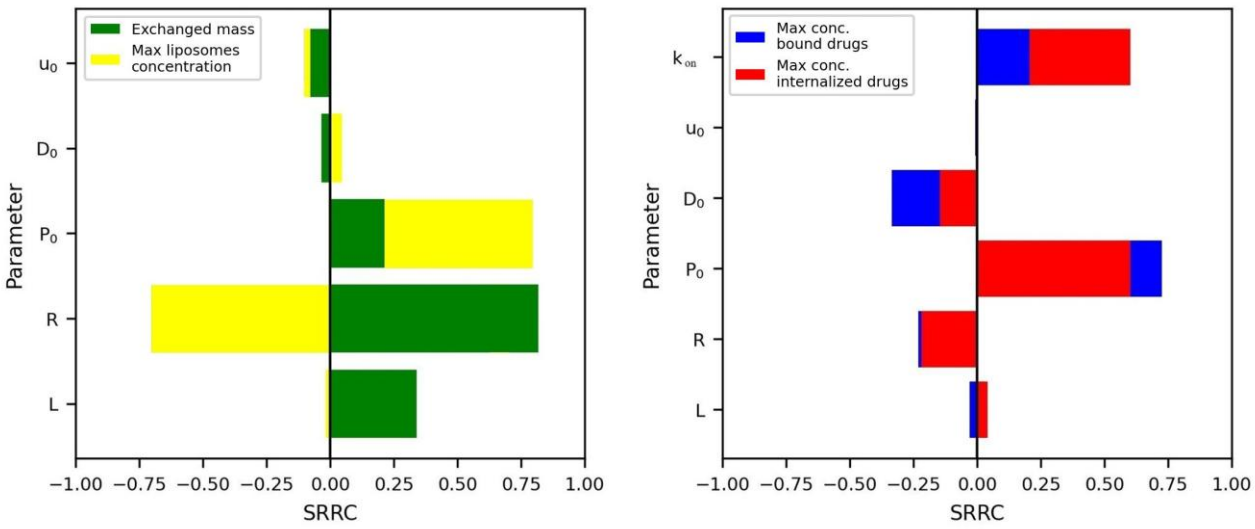

Figure 3: SRRCs values for the considered parameters.

The subscript "0" denotes baseline values, which are independent of temperature. On the left is shown the influence of the key parameters on the exchanged mass between the vascular compartment and the tissue compartment and on the maximum concentration, while on the right panel is presented the influence of the parameters on the maximum concentration of bound and internalized drugs. In the left panel of Figure 3, the sensitivity analysis indicates that certain parameters, namely blood velocity, the diffusivity coefficient, and Krogh cylinder length, exert minimal influence on the output maximum concentration function, suggesting that their variation does not substantially influence the maximum concentration of liposomes reached in the surrounding tissue. On the other hand, for parameters such as the length and the radius of the Krogh cylinder, it is evident that their variation has a prominent influence on the total exchanged mass between the two compartments, since, in this case, we are referring to variables that depend on the size of the computational domain. It is also interesting to notice that the microvascular permeability parameter has a positive influence on both the maximum concentration and the exchanged mass, since an increase in permeability enhances the passive diffusion through the vascular wall leading to a higher solute concentration in the tissue, thus, strategies to increase permeability (such as temperature increase) could potentially have benefits on the entire treatment. Conversely, a larger Krogh cylinder radius leads to a reduction in maximum concentration due to the greater volume available for solute distribution. In the right panel the effects of the key parameters on the concentration variables acting at cellular level are shown (Equations 6 and 7). Blood velocity does not directly influence the therapeutic action of the drugs, since it only slightly influences the amount of liposomes that are exchanged between the two compartment, in particular, as shown in the left panel, an increase in blood velocity slightly reduces the amount of drug that is transferred through the vascular wall, but it does not play any role in the binding and

internalization processes. As expected, an increase in the permeability coefficient represents a positive outcome for the therapeutic phenomena, increasing both the amount of bound and internalized drug, remarking again the need to further enhance the microvascular permeability to obtain better results from the treatment. To further elucidate the impact of individual parameters on the output functions, additional simulations were conducted in which each parameter was varied independently while the remaining parameters were held constant, equal to the baseline values presented in Table 1. The results from these simulations are displayed in Figure 4, offering a clearer visualization of each parameter's specific effect on the model outputs. For the sake of simplicity, in the following plots, the superscript "t" is dropped from the variables' symbols, since we will solely refer to the concentration in the tissue. All the plots show the space-averaged concentration of the liposomal concentration, the spatial distribution of the encapsulated drug is shown in Figure 5.

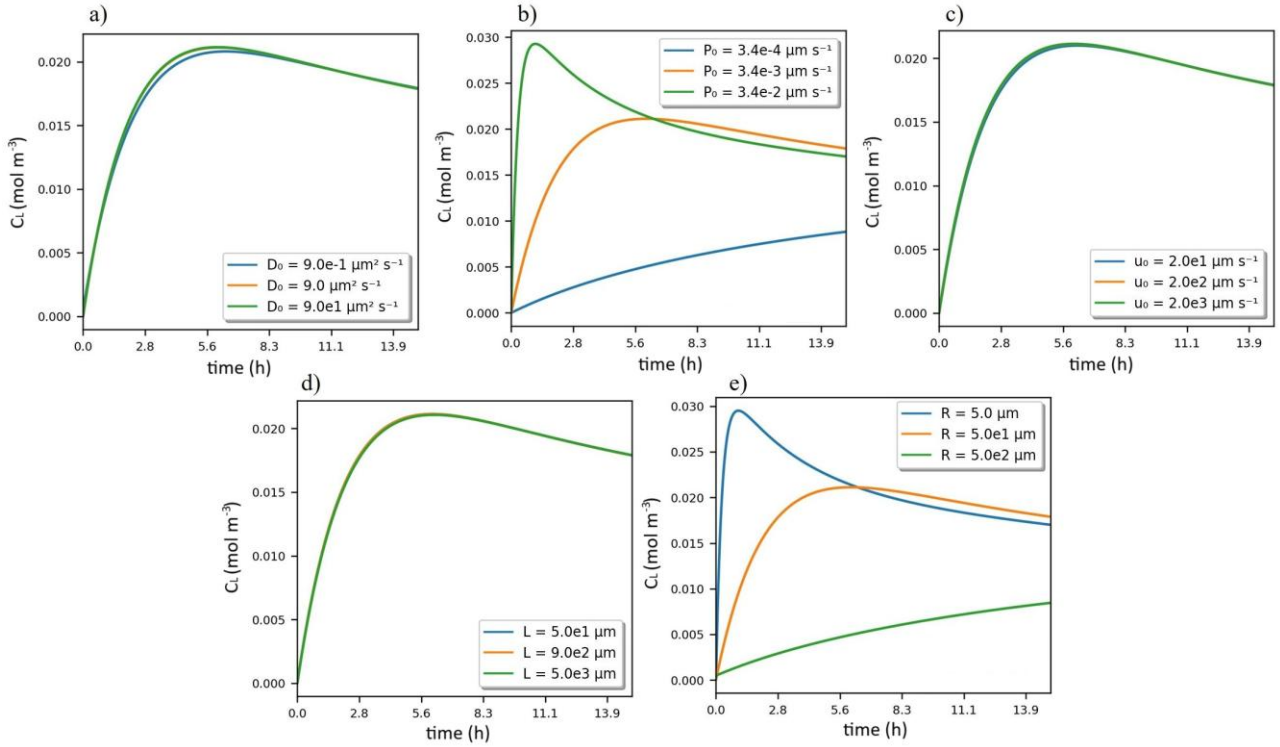

Figure 4: Influence of key model parameters on the average liposomes' concentration in tissue C_L. a) Diffusivity coefficient, b) Microvascular permeability, c) Blood velocity, d) Krogh cylinder length, e) Krogh cylinder radius.

To evaluate the robustness of the model, a local sensitivity analysis was performed using a One-at-a-Time (OAT) approach. Each input parameter was individually varied by relative to its baseline value (Table 2), while all other parameters remained fixed. This range was selected to encompass the typical physiological variance observed in solid tumors reported in literature.

As anticipated, the most substantial variation in tissue concentration is observed with changes in microvascular permeability, where increased permeability correlates with significantly improved drug penetration (Figure 4b). In contrast, no notable variations in tissue concentration were observed

with changes in blood velocity. Higher blood velocity values correspond to an increased blood flow rate; however, this does not significantly impact drug concentration in the tissue under the considered conditions. These results suggest that, for the considered model setting, passive diffusion is the driving transport mechanism [36]. Nevertheless, the impact of hyperthermia-induced vasodilation on drug delivery remains an area which needs further investigation, since vasodilation could potentially alter vascular wall permeability to drugs, which is not captured by the proposed model.

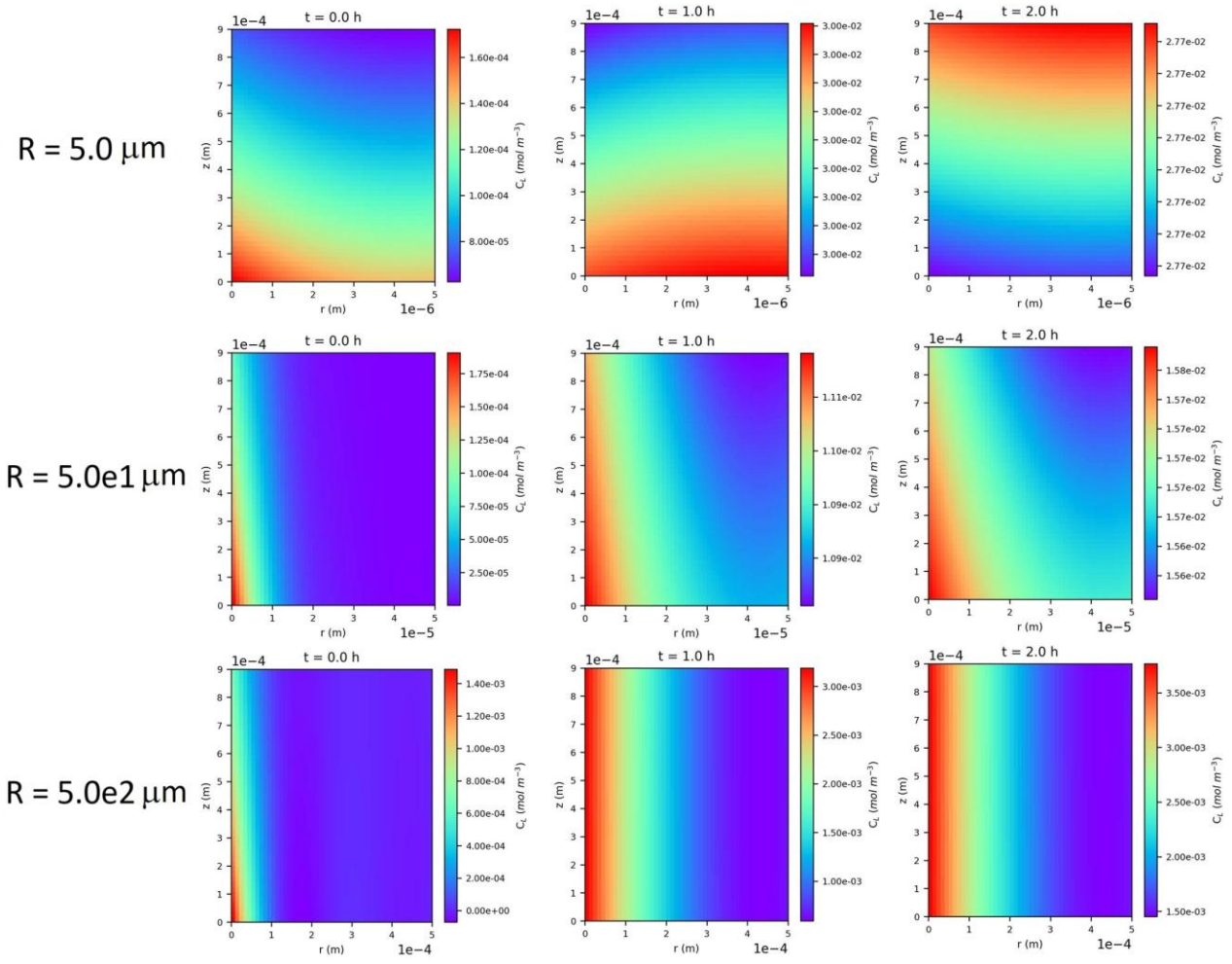

Figure 5: TSL concentration spatial distribution at different Krogh cylinder radii.

Figure 5 shows a 2-D representation of the liposomal doxorubicin distribution within the tissue surrounding the equivalent vessel. The simulation has been performed for three different values of the Krogh cylinder radius, and as expected also from the results of the sensitivity analysis (Figure 4) larger values of the Krogh cylinder radius lead to a more heterogeneous liposomes distribution. This analysis suggest that 0-D compartmental model can be successfully employed when analyzing tissue characterized by a high microvascular density (which translates into a lower size of the tissue cylinder) since the drug distribution is mostly uniform, while for less vascularized kind of tumor, which have a higher intercapillary distance, it is necessary to predict therapeutical outcome by

employing multi-dimensional model like the present one. However, for the following analysis, since the radius employed is equal to 50 μm, space-averaged concentration is considered since it becomes mostly uniform after the first two hours of treatment, as shown in Figure 5.

To further evaluate how the interstitial concentration of liposomes responds to variations in the injection protocol, an additional set of simulations was conducted. We considered other injection protocols by altering the parameters A_1 and A_2 of the curve describing the intravascular concentration function in Equation (6). The variability of these parameters, derived from the box plot in [20] and displayed in Figure 6, reflects the differences in intravascular concentration measured across a sample of seven patients, highlighting the patient-specific nature of the treatment response. This variability analysis enables a closer examination of how individual patient characteristics may influence drug delivery dynamics and informs the potential need for personalized adjustments to optimize therapeutic outcomes.

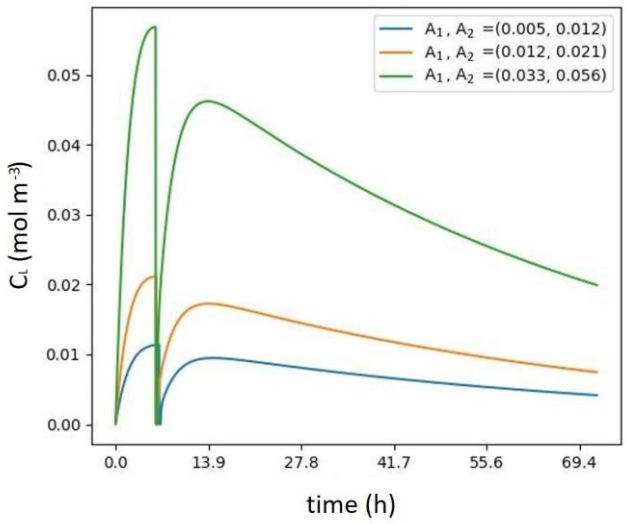

Figure 6: Impact of the injection protocol on the liposomes' tissue concentration.

The abrupt decline in tissue concentration observed at 5.6 hours post-injection is attributed to the start of the heating process, which triggers the release of the drug through the opening of the liposomes. This thermal activation facilitates the targeted delivery of the drug into the tissue, as the liposomes respond to the elevated temperature by releasing their payload, thereby causing a marked decrease in their concentration within the interstitial space.

While this section focuses on the sensitivity of mass transport and geometric parameters, it is important to note that the system's sensitivity to temperature elevation and heating schedules is intrinsically evaluated in the following Section 3.2. Furthermore, within the proposed 1-D Krogh cylinder framework, the convective transport of the drug is governed by the capillary blood velocity (u), which is included in the sensitivity analysis (Figures 4 and 5), whereas the macroscopic tissue

perfusion rate (ω) primarily acts as a heat sink in the bioheat formulation (Equation 8). Finally, the drug release rate (k_{rel}) is modeled as a piecewise threshold function based on established literature (Equation 9); since TSLs are engineered to release their payload almost instantaneously upon reaching the 42°C threshold, a parametric variation of the release kinetics would not add physiological significance to this specific macroscopic analysis.

3.2 *Impact of heating schedule on drug concentration*

To assess the reliability of the present model, we present an overall analysis of the treatment in Figure 7, which shows results similar to those in previous works [21], [9].

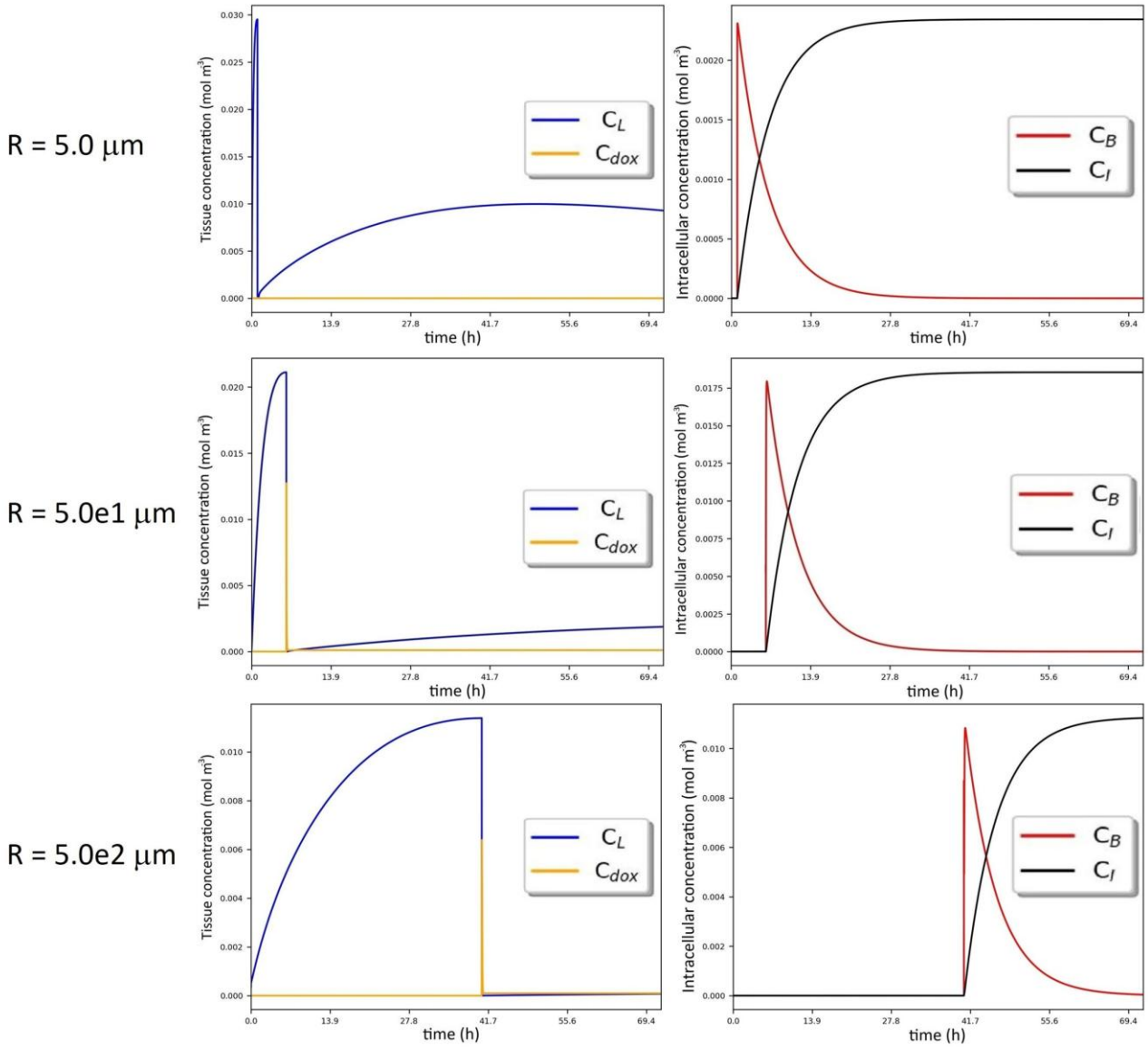

Figure 7: Heat triggered drug release chemotherapeutic treatment. Variation of liposomal and drug concentration in tissue over time.

In Figure 7, the left panels show the interstitial concentrations of both liposomes and free doxorubicin for the three tested Krogh cylinder sizes, following the release event triggered by hyperthermic conditions, while the right panels display the bound and internalized concentrations of doxorubicin. These profiles are presented separately, as they represent two distinct compartments, namely, tissue and intracellular compartment, each governed by a different set of equations within the model (eq. 4-7). Drug release from liposomes occurs because of thermal activation when interstitial concentrations of liposomes reach their peak. However, the primary therapeutic impact of the treatment is associated with the level of internalized doxorubicin, which interacts directly with tumoral cells. The trends observed in these concentration curves align with patterns previously described in prior studies [21], [9], [10], which are referenced here for a more detailed explanation of the mechanisms involved. In summary, after the injection and the subsequent transport of TSL from the vascular compartment to the tissue compartment, the concentration of TSL (blue curve) increases. When it reaches its maximum concentration (occurring at approximately 5.6 hours after injection if no preheating treatment is delivered), the hyperthermia treatment is performed. When the temperature level exceeds 42°C, the liposomes immediately release their payload, and this phenomenon translates to the abrupt decrease in their concentration. On the other hand, the concentration of free doxorubicin in the tissue compartment increases (orange curve) and reaches its peak a few minutes after the release from the TSL. However, due to the high binding affinity of doxorubicin (highlighted by the high value for the constant of binding rate k_{on} in Table 1), most of the free molecules binds to cancer cells, rapidly increasing the concentration of bound drugs in the cellular compartment (red curve in the right panel plot). Due to the internalization mechanism, bound drugs subsequently get internalized by cancer cells, increasing the internalized doxorubicin concentration (black curve), which has the therapeutically relevant action. From the figure, it is evident that by changing the size of the Krogh cylinder the amount of drug that is transferred from the vascular compartment to the tissue is different. For increasing size of the Krogh cylinder the liposomes concentration in tissue decreases, aligning these results with the ones observed through the spatial distribution analysis. This phenomenon suggests that this kind of treatment could vary its performance depending on the type of tissue involved. These results suggest that the present model can be employed to predict the overall outcomes of the treatment by choosing a feasible cylinder radius depending on the tissue characteristics.

The flexibility of the current numerical model enables efficient exploration of strategies to enhance drug internalization. The influence of temperature elevation on interstitial drug diffusion during treatment is a central focus of this work, addressing a gap in the current literature where such thermally mediated effects have not been comprehensively quantified. By incorporating temperature-

dependent parameters (Equations 10 to 12), the model allows for a simulation that specifically evaluates the impact of temperature on interstitial concentration over a treatment duration of 15 hours. The results, displayed in Figure 8, demonstrate how tissue heating significantly enhances drug diffusion.

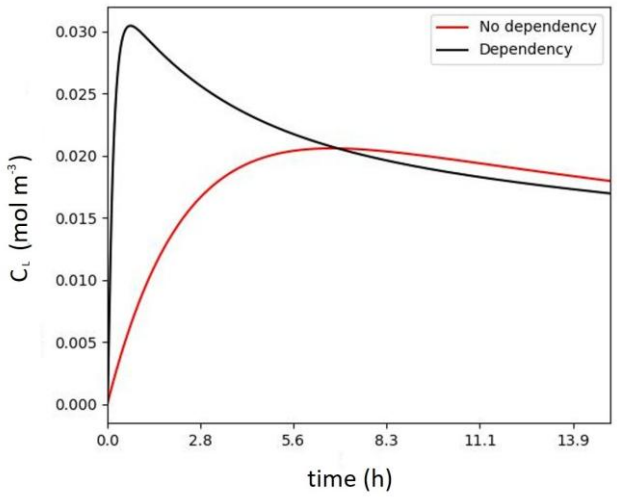

Figure 8: Influence of temperature on the interstitial concentration of liposomes in tissue.

In this scenario, thermal energy 'generation' is assumed to be sustained for the entire simulation period, although at a lower intensity to maintain tissue temperature below the threshold necessary for drug release initiation. The data indicate that mild hyperthermia conditions enhance peak tissue concentration of TSL by approximately 50%. This notable increase is attributed to improved microvascular permeability induced by the mild heating, which in turn promotes greater drug penetration into the surrounding tissue. The findings suggest that implementing a controlled, preliminary heating phase prior to the main treatment could enhance the therapeutic outcome by conditioning the tissue for optimal drug delivery [37]. Importantly, this approach requires careful monitoring to maintain tissue temperature below the critical threshold to avoid vascular shut-down and tissue damage, which could impede transvascular transport.

In this study, preheating is modeled by simulating a preliminary heating schedule during the first minutes of the treatment with a significantly lower heat generation (3.5e5 W m^{-3}). However, while choosing the heating power for the preheating phase, it is necessary to account for the thermal damage induced by high temperature that could hinder the drug transport within the tissue [38]. To account for this phenomenon, the functions employed to describe the microvascular permeability and the diffusivity coefficient have been modified by implementing a dependency with the probability of

thermal damage θ. The probability of thermal damage is computed through the Arrhenius kinetics equation [39]:

$$P(T,\theta) = P(T)(1-\theta) \tag{15}$$

$$D(T,\theta) = D(T)(1-\theta) \tag{16}$$

$$\theta = 1 - \exp\left(-\Omega(t)\right) \tag{17}$$

$$\Omega(t) = \int_0^t A\exp\left(-\frac{\Delta E}{R_g T(\tau)}\right) d\tau \tag{18}$$

where A (s^{-1}) is the frequency factor, ΔE (J mol^{-1}) the activation energy for the irreversible transformation, referred to the tumor liver tissue. In this case A = 3.247e47 s^{-1} and ΔE = 2.814e5 (J mol^{-1}) [9], R_g (J mol^{-1} K^{-1}) the universal gas constant and T the tissue temperature. Several heating schedules have been tested, considering increasing preheating duration. The results are shown in Figure 9.

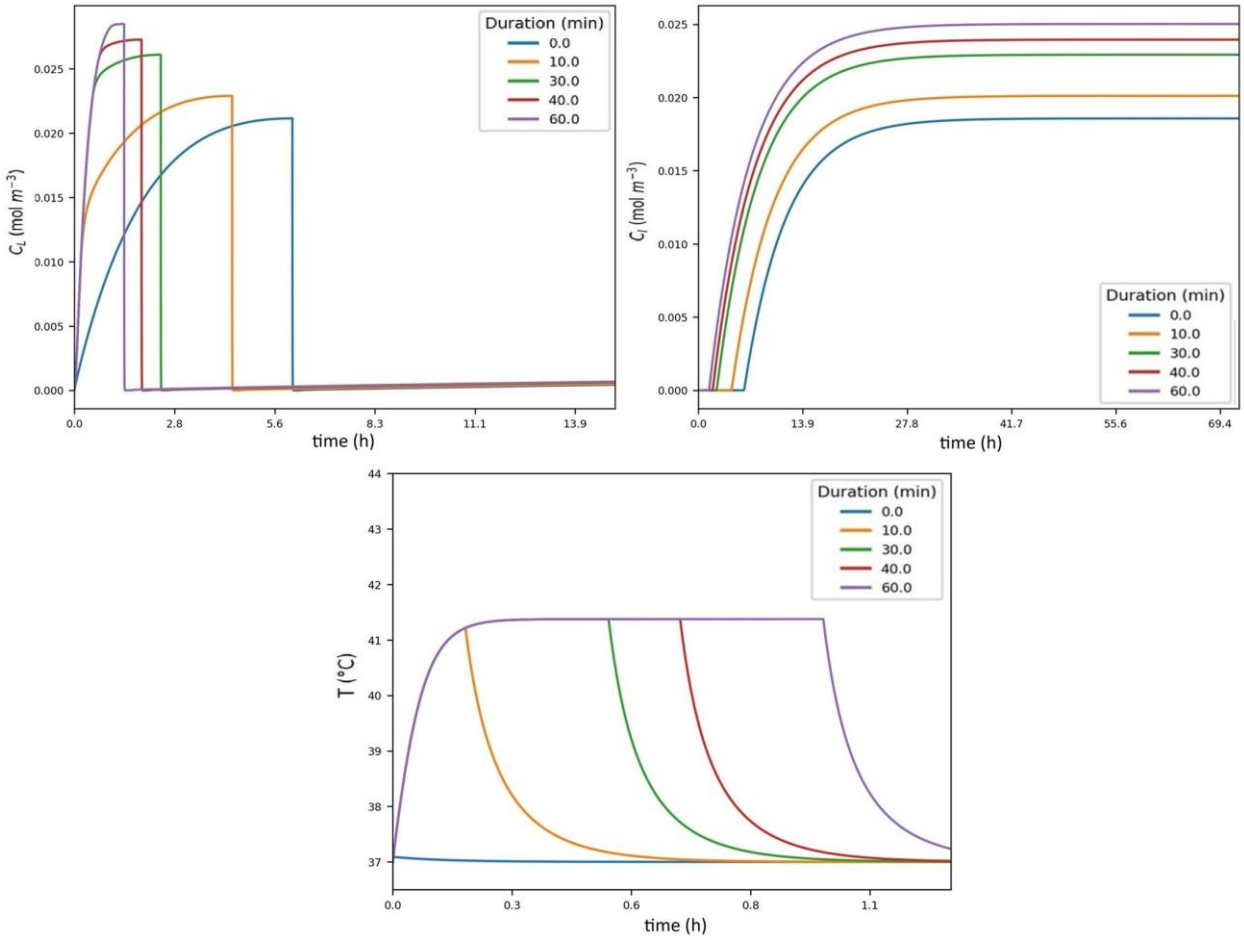

Figure 9: Left panel: liposomes tissue concentration for different preheating schedules. Right panel: Internalized doxorubicin concentration. Below: temperature profiles corresponding to the tested preheating durations.

As shown in the figures, a preliminary temperature increase through mild hyperthermia can enhance both TSL diffusion and doxorubicin internalization. Simulations indicate that the lower thermal energy generation, compared to the level required to trigger TSL, does not cause excessive thermal damage that could hinder drug diffusion. Instead, the beneficial effects of increased temperature on permeability and diffusivity significantly outweigh any potential drawbacks. Since this treatment falls under the mild-hyperthermia modality, minimizing thermal damage to tissues is crucial. Although a one-hour preheating treatment appears to provide the best therapeutic outcome, a shorter duration is preferable to reduce any potential risk of thermal damage in a real world-scenario, requiring a trade-off decision.

As shown in Figure 9, a 30-minute preheating treatment allows the enhancement of the therapeutic outcome, increasing the internalized concentration of doxorubicin by 29.4% with respect to the treatment without preheating, while maintaining a necrosis probability of 0.05. This probability is lower compared to the 60 minutes duration that increases the necrosis probability during the pre-heating treatment up to 0.21, while offering a relatively marginal improvement in the internalized drug concentration, compared to the 30 minutes preheating treatment.

In summary, these findings highlight the importance of temperature modulation in optimizing drug delivery to solid tumors, where controlled heating can significantly improve drug accessibility to tumor cells, increasing the likelihood of therapeutic success. This model provides a valuable tool for exploring the dynamics of heat-augmented drug delivery, offering insights that may support the development of patient-specific treatment protocols aimed at maximizing drug efficacy while minimizing adverse effects associated with excessive tissue heating.

4. Conclusions

This study presents a novel 1-D computational model for hyperthermia-controlled drug delivery, offering a computationally efficient alternative to existing three-dimensional models. By integrating the Krogh cylinder framework with temperature-dependent parameters, the model effectively captures the influence of hyperthermia on drug release and distribution. Sensitivity analysis highlights the critical role of microvascular permeability and tissue diffusivity in enhancing drug transport. A key finding of this study is that preheating the tissue before TSL administration improves drug accumulation and internalization, with a 30-minute preheating period increasing intracellular doxorubicin by 29.4%. This strategy enhances therapeutic efficacy while minimizing thermal damage risks.

To ensure the reliability of the proposed mathematical framework, the 1-D model was successfully verified against established 0-D compartmental models from the literature, demonstrating excellent mathematical agreement in predicting baseline tissue liposome concentrations. Furthermore, the simulated interstitial and intracellular drug concentration profiles under hyperthermic conditions align consistently with previously published theoretical trends, providing strong confidence in the model's predictive capabilities even in the absence of direct *in vivo* experimental validation.

While the proposed 1-D Krogh cylinder framework offers significant computational efficiency, several limitations regarding geometrical and physiological idealizations must be acknowledged. First, the model relies on a periodic, homogeneous vascular arrangement. This idealization neglects the chaotic tortuosity and branching hierarchies characteristic of *in vivo* tumor vasculature, potentially underestimating specific regions of vascular stasis or arteriolar shunting. Second, regarding mass transport, the formulation assumes that interstitial transport is dominated by diffusion, thereby neglecting convective fluxes. This assumption is supported by the high interstitial fluid pressure (IFP) observed in solid tumors, which minimizes transvascular pressure gradients; however, this approach may be less accurate at the tumor periphery where pressure gradients persist. Furthermore, the model explicitly omits active lymphatic drainage. While functional lymphatics are often collapsed in the tumor core due to high IFP, their presence at the tumor margin plays a role in fluid balance that is not captured here. Third, the bioheat model assumes a uniform specific absorption rate (SAR), which does not account for the dielectric heterogeneity of complex tissue structures. Finally, cellular-level heterogeneity is averaged into effective continuum properties (e.g., diffusivity, binding), meaning the model predicts macroscopic tissue trends rather than discrete, single-cell pharmacokinetics.

Future research should focus on extending this framework to patient-specific tumor environments and validating predictions with *in vivo* data. Additionally, the inclusion of more complex vascular architectures and patient-specific parameters could further refine the accuracy of the model. Experimental validation through controlled hyperthermia treatments and drug delivery trials will be essential to confirm the model’s predictions and its clinical applicability. The computational efficiency of this model also makes it a valuable tool for real-time treatment planning, allowing for adaptive strategies based on tumor response. Furthermore, exploring the effects of alternative heating protocols and different types of thermosensitive drug carriers could provide deeper insights into optimizing hyperthermia-assisted chemotherapy.

To implement this framework clinically, input parameters must be derived from non-invasive imaging data. Patient-specific tumor geometry (radius) is readily available via segmentation of structural MRI or CT scans. Transport parameters, such as vascular permeability and interstitial diffusivity, can be estimated using Dynamic Contrast-Enhanced MRI (DCE-MRI) and Diffusion Tensor Imaging (DTI),

respectively. While direct measurement of interstitial fluid pressure remains invasive, this model allows for the inverse estimation of hydraulic conductivity by fitting the model outputs to time-resolved imaging data.

The transition from this reduced-order 1-D model to adaptive clinical planning requires addressing the trade-off between geometric fidelity and computational speed. High-fidelity 3D Computational Fluid Dynamics (CFD) models capture complex tumor heterogeneity but often require hours or days of computation, rendering them unsuitable for real-time sensitivity analysis or iterative treatment optimization. In contrast, the proposed 1-D model serves as a compartmental surrogate, prioritizing computational efficiency. This speed is critical for "real-time" planning: it allows the system to run inverse algorithms that fit the model to patient data, or to run Monte Carlo simulations to predict treatment uncertainty. Therefore, while this model simplifies spatial geometry, it provides a necessary bridge for converting static imaging data into dynamic transport predictions at the point of care.

Ethics statement

The authors declare that the study was conducted in accordance with the ethical standards of the relevant institutional and/or national research committee, and with the 1964 Helsinki declaration and its later amendments or comparable ethical standards. All participants provided informed consent prior to their inclusion in the study. This research did not involve any studies with human participants or animals performed by any of the authors.

References

[1] Khleif S. N., Rixie O., Skeel R. T., 'Skeel's Handbook of Cancer Therapy'. Lippincott Williams & Wilkins, 9th Ed., 2016.

[2] A. Andreozzi, L. Brunese, M. Iasiello, C. Tucci, and G. P. Vanoli, 'Modeling Heat Transfer in Tumors: A Review of Thermal Therapies', *Ann. Biomed. Eng.*, vol. 47, no. 3, pp. 676–693, Mar. 2019, doi: 10.1007/s10439-018-02177-x.

[3] C. Brace, 'Thermal Tumor Ablation in Clinical Use', *IEEE Pulse*, vol. 2, no. 5, pp. 28–38, Sep. 2011, doi: 10.1109/MPUL.2011.942603.

[4] T. Ta and T. M. Porter, 'Thermosensitive liposomes for localized delivery and triggered release of chemotherapy', *J. Control. Release Off. J. Control. Release Soc.*, vol. 169, no. 1–2, pp. 112–125, Jul. 2013, doi: 10.1016/j.jconrel.2013.03.036.

[5] M. Alawak, A. A. Dayyih, I. Awak, B. Gutberlet, K. Engelhardt, and U. Bakowsky, 'Magnetic Thermosensitive Liposomes Loaded with Doxorubicin', *Methods Mol. Biol. Clifton NJ*, vol. 2622, pp. 103–119, 2023, doi: 10.1007/978-1-0716-2954-3_9.

[6] M. Chaudhry, P. Lyon, C. Coussios, and R. Carlisle, 'Thermosensitive liposomes: a promising step toward localised chemotherapy', *Expert Opin. Drug Deliv.*, vol. 19, no. 8, pp. 899–912, Aug. 2022, doi: 10.1080/17425247.2022.2099834.

[7] M. H. H. Tehrani, M. Soltani, F. Moradi Kashkooli, M. Mahmoudi, and K. Raahemifar, 'Computational Modeling of Combination of Magnetic Hyperthermia and Temperature-Sensitive Liposome for Controlled

Drug Release in Solid Tumor', *Pharmaceutics*, vol. 14, no. 1, p. 35, Dec. 2021, doi: 10.3390/pharmaceutics14010035.
[8] W. Zhan and X. Y. Xu, 'A Mathematical Model for Thermosensitive Liposomal Delivery of Doxorubicin to Solid Tumour', *J. Drug Deliv.*, vol. 2013, pp. 1–13, Jan. 2013, doi: 10.1155/2013/172529.
[9] G. Adabbo, A. Andreozzi, M. Iasiello, P. A. Netti, and G. P. Vanoli, 'A 3D numerical model of controlled drug delivery to solid tumor by means of mild microwave hyperthermia-activated thermo-sensitive liposomes', *Int. J. Therm. Sci.*, vol. 193, p. 108528, Nov. 2023, doi: 10.1016/j.ijthermalsci.2023.108528.
[10] G. Adabbo, A. Andreozzi, M. Iasiello, and G. P. Vanoli, 'Numerical evaluation of heat-triggered drug release via thermo-sensitive liposomes: A comparison between image-based vascularized tumor and volume-averaged porous media models', *Int. J. Heat Mass Transf.*, vol. 220, p. 124942, Mar. 2024, doi: 10.1016/j.ijheatmasstransfer.2023.124942.
[11] A. W. El-Kareh and T. W. Secomb, 'A Mathematical Model for Comparison of Bolus Injection, Continuous Infusion, and Liposomal Delivery of Doxorubicin to Tumor Cells', *Neoplasia*, vol. 2, no. 4, pp. 325–338, Jul. 2000, doi: 10.1038/sj.neo.7900096.
[12] T. W. Secomb, 'Krogh-cylinder and infinite-domain models for washout of an inert diffusible solute from tissue', *Microcirc. N. Y. N 1994*, vol. 22, no. 1, pp. 91–98, Jan. 2015, doi: 10.1111/micc.12180.
[13] X. Qiu, 'Fluid flow in a Krogh cylinder: A model for a single capillary and surrounding tissue'.
[14] A. Coccarelli, E. Boileau, D. Parthimos, and P. Nithiarasu, 'An advanced computational bioheat transfer model for a human body with an embedded systemic circulation', *Biomech. Model. Mechanobiol.*, vol. 15, no. 5, pp. 1173–1190, Oct. 2016, doi: 10.1007/s10237-015-0751-4.
[15] T. W. Secomb, 'Krogh-cylinder and infinite-domain models for washout of an inert diffusible solute from tissue', *Microcirc. N. Y. N 1994*, vol. 22, no. 1, pp. 91–98, Jan. 2015, doi: 10.1111/micc.12180.
[16] D. Fukumura, D. G. Duda, L. L. Munn, and R. K. Jain, 'Tumor Microvasculature and Microenvironment: Novel Insights Through Intravital Imaging in Pre-Clinical Models', *Microcirc. N. Y. N 1994*, vol. 17, no. 3, pp. 206–225, Apr. 2010, doi: 10.1111/j.1549-8719.2010.00029.x.
[17] L. Qin and J. M. Crawford, '1 - Anatomy and Cellular Functions of the Liver', in *Zakim and Boyer's Hepatology (Seventh Edition)*, A. J. Sanyal, T. D. Boyer, K. D. Lindor, and N. A. Terrault, Eds., Philadelphia: Elsevier, 2018, pp. 2-19.e4. doi: 10.1016/B978-0-323-37591-7.00001-X.
[18] P. A. Netti, L. T. Baxter, Y. Boucher, R. Skalak, and R. K. Jain, 'Time-dependent behavior of interstitial fluid pressure in solid tumors: implications for drug delivery', *Cancer Res.*, vol. 55, no. 22, pp. 5451–5458, Nov. 1995.
[19] L. T. Baxter, R. K. Jain, and E. Svensjö, 'Vascular permeability and interstitial diffusion of macromolecules in the hamster cheek pouch: effects of vasoactive drugs', *Microvasc. Res.*, vol. 34, no. 3, pp. 336–348, Nov. 1987, doi: 10.1016/0026-2862(87)90066-5.
[20] A. Gabizon, R. Catane, B. Uziely, B. Kaufman, T. Safra, R. Cohen, F. Martin, A. Huang, and Y. Barenholz, 'Prolonged circulation time and enhanced accumulation in malignant exudates of doxorubicin encapsulated in polyethylene-glycol coated liposomes', *Cancer Res.*, vol. 54, no. 4, pp. 987–992, Feb. 1994.
[21] T. Stylianopoulos, E.-A. Economides, J. W. Baish, D. Fukumura, and R. K. Jain, 'Towards Optimal Design of Cancer Nanomedicines: Multi-stage Nanoparticles for the Treatment of Solid Tumors', *Ann. Biomed. Eng.*, vol. 43, no. 9, pp. 2291–2300, Sep. 2015, doi: 10.1007/s10439-015-1276-9.
[22] H. H. Pennes, 'Analysis of Tissue and Arterial Blood Temperatures in the Resting Human Forearm', *J. Appl. Physiol.*, vol. 1, no. 2, pp. 93–122, Aug. 1948, doi: 10.1152/jappl.1948.1.2.93.
[23] Y. Du, N. Li, and M. Long, 'Chapter 6 - Liver sinusoid on a chip', in *Methods in Cell Biology*, vol. 146, J. Doh, D. Fletcher, and M. Piel, Eds., in Microfluidics in Cell Biology Part A: Microfluidics for Multicellular Systems, vol. 146. , Academic Press, 2018, pp. 105–134. doi: 10.1016/bs.mcb.2018.06.002.
[24] P. Yuan, 'Numerical analysis of an equivalent heat transfer coefficient in a porous model for simulating a biological tissue in a hyperthermia therapy', *Int. J. Heat Mass Transf.*, vol. 52, no. 7–8, pp. 1734–1740, Mar. 2009, doi: 10.1016/j.ijheatmasstransfer.2008.09.033.
[25] T. L. Bergman, A. S. Lavine, F. P. Incropera, and D. P. DeWitt, *Fundamentals of Heat and Mass Transfer*, 8th ed. New York: Wiley, 2017.
[26] Y. Huang, B. Gu, C. Liu, J. Stebbing, W. Gedroyc, M. Thanou, and X. Y. Xu, 'Thermosensitive Liposome-Mediated Drug Delivery in Chemotherapy: Mathematical Modelling for Spatio–temporal Drug Distribution and Model-Based Optimisation', *Pharmaceutics*, vol. 11, no. 12, p. 637, Nov. 2019, doi: 10.3390/pharmaceutics11120637.

[27] J. J. Bosque, G. F. Calvo, V. M. Pérez-García, and M. C. Navarro, ‘The interplay of blood flow and temperature in regional hyperthermia: a mathematical approach’, *R. Soc. Open Sci.*, vol. 8, no. 1, p. 201234, Jan. 2021, doi: 10.1098/rsos.201234.
[28] M. Dewhirst, J. F. Gross, D. Sim, P. Arnold, and D. Boyer, ‘The effect of rate of heating or cooling prior to heating on tumor and normal tissue microcirculatory blood flow’, *Biorheology*, vol. 21, no. 4, pp. 539–558, 1984, doi: 10.3233/bir-1984-21413.
[29] C. Eipel, K. Abshagen, and B. Vollmar, ‘Regulation of hepatic blood flow: The hepatic arterial buffer response revisited’, *World J. Gastroenterol. WJG*, vol. 16, no. 48, pp. 6046–6057, Dec. 2010, doi: 10.3748/wjg.v16.i48.6046.
[30] J.-Y. Zhu, X.-S. Leng, N. Dong, G.-Y. Qi, and R.-Y. Du, ‘Measurement of liver volume and its clinical significance in cirrhotic portal hypertensive patients’, *World J. Gastroenterol.*, vol. 5, no. 6, pp. 525–526, Dec. 1999, doi: 10.3748/wjg.v5.i6.525.
[31] Q. Chen, A. Krol, A. Wright, D. Needham, M. W. Dewhirst, and F. Yuan, ‘Tumor microvascular permeability is a key determinant for antivascular effects of doxorubicin encapsulated in a temperature sensitive liposome’, *Int. J. Hyperth. Off. J. Eur. Soc. Hyperthermic Oncol. North Am. Hyperth. Group*, vol. 24, no. 6, pp. 475–482, Sep. 2008, doi: 10.1080/02656730701854767.
[32] M. Dunne, M. Regenold, and C. Allen, ‘Hyperthermia can alter tumor physiology and improve chemo- and radio-therapy efficacy’, *Adv. Drug Deliv. Rev.*, vol. 163–164, pp. 98–124, Jan. 2020, doi: 10.1016/j.addr.2020.07.007.
[33] N. Z. Wu, D. Da, T. L. Rudoll, D. Needham, A. R. Whorton, and M. W. Dewhirst, ‘Increased microvascular permeability contributes to preferential accumulation of Stealth liposomes in tumor tissue’, *Cancer Res.*, vol. 53, no. 16, pp. 3765–3770, Aug. 1993.
[34] C. Tucci, M. Trujillo, E. Berjano, M. Iasiello, A. Andreozzi, and G. P. Vanoli, ‘Mathematical modeling of microwave liver ablation with a variable-porosity medium approach’, *Comput. Methods Programs Biomed.*, vol. 214, p. 106569, Feb. 2022, doi: 10.1016/j.cmpb.2021.106569.
[35] A. A. Stokhof and A. D. Rick, ‘Chapter 10 - Circulatory system’, in *Medical History and Physical Examination in Companion Animals (Second Edition)*, A. Rijnberk, F. J. van Sluijs, B. E. Belshaw, B. Janssen, J. Fama, E. Teske, M. J. A. Mudde, E. Schaefers, R. N. van Blokland, and Y. W. E. A. Pollak, Eds., Edinburgh: W.B. Saunders, 2009, pp. 75–85. doi: 10.1016/B978-0-7020-2968-4.00010-1.
[36] N. Herring and D.J. Paterson, 'Levick's Introduction to Cardiovascular Physiology' (6th ed.), CRC Press, 2018, doi: 10.1201/9781351107754
[37] G. Adabbo, A. Andreozzi, M. Iasiello, G. Napoli, and G. P. Vanoli, ‘A multi-objective optimization framework through genetic algorithm for hyperthermia-mediated drug delivery’, *Comput. Biol. Med.*, vol. 189, p. 109895, May 2025, doi: 10.1016/j.compbiomed.2025.109895.
[38] M. Regenold, P. Bannigan, J. C. Evans, A. Waspe, M. J. Temple, and C. Allen, ‘Turning down the heat: The case for mild hyperthermia and thermosensitive liposomes’, *Nanomedicine Nanotechnol. Biol. Med.*, vol. 40, p. 102484, Feb. 2022, doi: 10.1016/j.nano.2021.102484.
[39] A. Andreozzi, M. Iasiello, and C. Tucci, ‘An overview of mathematical models and modulated-heating protocols for thermal ablation’, in *Advances in Heat Transfer*, vol. 52, Elsevier, 2020, pp. 489–541. doi: 10.1016/bs.aiht.2020.07.003.